chemosensors

MDPI

Article

Facile One-Pot Synthesis of Au/Ag Bimetallic Nanoclusters as a Fluorescent Probe for the Detection of Hg^{2+} and Cu^{2+}

Hongbo Lin [1,2], Taiqun Yang [1,3,*], Lei Li [1,3] and Lang Liu [1,3,*]

[1] School of Science, Jiangnan University, Wuxi 214122, China
[2] Changxin Xinqiao Storage Technology Co., Ltd., No. 2788, Xinhuai Avenue, Hefei 230000, China
[3] Jiangsu Provincial Research Center of Light Industrial Optoelectronic Engineering and Technology, Lihu Avenue 1800, Wuxi 214122, China
* Correspondence: tqyang@jiangnan.edu.cn (T.Y.); liulang@jiangnan.edu.cn (L.L.)

Abstract

Fluorescent metal nanoclusters show great promise in heavy metal ion sensing. Herein, a bimetallic nanocluster (GSH-Au/Ag NCs) with orange fluorescence was synthesized through a facile one-pot method. The synthesized GSH-Au/Ag NCs displayed optimal excitation and emission peaks at 275 and 610 nm, respectively. The incorporation of silver can enhance the fluorescence of metal nanoclusters. The fluorescence of as-synthesized GSH-Au/Ag NCs can be significantly quenched by Hg^{2+} and Cu^{2+}, and a "on–off" fluorescent probe was designed. The detection conditions, including pH and the concentration of the probe, were optimized. The respective detection limits for Hg^{2+} and Cu^{2+} ions under optimal detection conditions are estimated to be 40 nM and 33 nM, over the linear range of 100–1200 nM. Furthermore, a ratiometric fluorescent probe was prepared by mixing quinine sulfate and as-synthesized GSH-Au/Ag NCs. Hg^{2+} and Cu^{2+} can effectively quench the red fluorescence of GSH-Au/Ag NCs, whereas the blue fluorescence of quinine sulfate remains invariant. This leads to measurable changes in the RGB values of the resulting fluorescence images. The ratio (R/B) exhibits a linear relationship with the concentration of Hg^{2+} and Cu^{2+}, enabling the determination of its concentration by analyzing RGB values in fluorescence images. This visual detection method significantly reduces both assay time and cost, making it suitable for on-site detection of heavy metal ions in water samples.

Keywords: nanoclusters; fluorescent probe; visual detection

1. Introduction

In recent years, with the rapid development of industrial and agricultural activities, heavy metal ion pollution has become increasingly severe [1–3]. Approximately 14–17% of global arable land is contaminated by heavy metals. These ions can enter and accumulate in biological systems through the food chain, causing serious harm [4–7]. For instance, mercury ions (Hg^{2+}) exhibit strong neurotoxicity and nephrotoxicity, can cross the blood–brain barrier, and lead to memory impairment, emotional instability, tremors, and central nervous system damage, particularly significant in harming fetal neural development [8,9]. Copper ions (Cu^{2+}) are less toxic than mercury ions. However, their extensive use in industries such as electronic and mechanical manufacturing results in significant release of Cu^{2+} into the environment through industrial waste and emissions. Copper ions are essential trace elements for the human body in appropriate amounts but become significantly toxic when present in excess, potentially damaging the liver, nervous system, kidneys, and hematological system [10–12]. Therefore, it is of urgent practical significance to develop simple

Check for updates

Received: 14 February 2026
Revised: 17 March 2026
Accepted: 23 March 2026
Published: 25 March 2026

Copyright: © 2026 by the authors. Licensee MDPI, Basel, Switzerland. This article is an open access article distributed under the terms and conditions of the Creative Commons Attribution (CC BY) license.

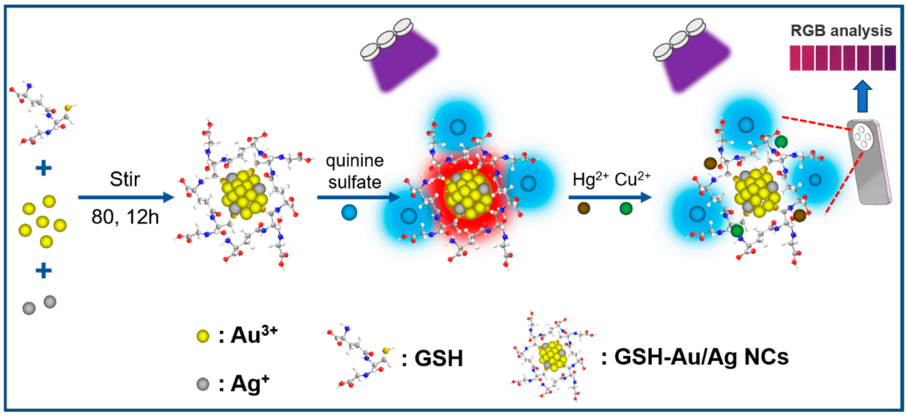
and sensitive methods for detecting Hg^{2+} and Cu^{2+} in water bodies. At present, there are some commonly used methods for the sensitive detection of heavy metal ions, including atomic absorption/emission spectrometry (AAS/AES) [13–15], inductively coupled plasma mass spectrometry (ICP–MS) [16–18], and electrochemical methods [19,20]. Although these methods exhibit high sensitivity for metal ion detection, they typically require extensive sample pretreatment, face high instrumentation costs, and lack portability, collectively hindering rapid on-site analysis.

Recently, fluorescence spectroscopy technology has been widely used for the detection of heavy metal ions because it offers high sensitivity, good selectivity, rapid analysis, non-destructive testing, and minimal sample consumption [21–23]. In this regard, many fluorescent materials, including traditional fluorescent dyes, inorganic semiconductor quantum dots (QDs) and carbon dots (CDs), have been widely employed in the fabrication of fluorescent probes for heavy metal ion detection [24–26]. Metal nanoclusters (MNCs) are a new class of fluorescent material with a lot of appealing properties, such as large Stokes shift, good biocompatibility and excellent photostability, which have attracted intense attention for the construction of fluorescent sensing platforms for the determination of heavy metal ions [7,27]. Benavides et al. reported an in situ metal reduction strategy for the fabrication of copper nanoclusters using multithiolated polymer as template [28]. The fluorescence of as-fabricated copper nanoclusters can be specifically quenched by $Hg^{2+,}$ and a "switch-off" fluorescent probe was designed, with a linear response range of 0–100 μM. Chen et al. established a ratiometric fluorescence method for sensitive detection of Hg^{2+} using a gold nanocluster/carbon quantum dot (AuNC/CQD) nanohybrid probe [8]. The linear response range is from 0.8 to 77 μM, and the LOD is 0.36 μM. Yu et al. designed a ratiometric fluorescent probe by the conjugation of red-emitting Au-GSH NCs and green-emitting FITC [9]. The probe was used for rapid sensing and imaging of Hg^{2+} in living cells and zebrafish with high contrast. The linear response range is 0–20 μM, and the LOD is calculated to be 0.5 μM. Hao et al. synthesized a dual-emission fluorescent sensor using one-pot encapsulation of Tb(III) and GSH-Cu NCs into metal–organic frameworks (MOFs) [29]. The fluorescence of Tb^{3+} is significantly quenched by Cu^{2+}, whereas that of Cu NCs remains unchanged. The determination of Cu^{2+} can be accomplished by measuring the ratio of fluorescence intensity at 450 nm to 548 nm. The linear response range is 1–30 μM, and the LOD is 178 nM. Youn et al. designed simple tripeptides to form fluorescent Au NCs [30]. The number of tyrosine residues influences the probe's response to Cu^{2+} and Fe^{3+}. Fluorescence quenching arises from the chelation between surface peptides and metal ions, which induces aggregation of the clusters. The linear range for Cu^{2+} and Fe^{3+} is 0.25–25 μM (LOD = 0.77 μM) and 0.25–100 μM (LOD = 3.2 μM), respectively.

The fluorescence performance of MNCs is of crucial importance for their applications in the field of fluorescence probes. Metal doping is an effective approach to modulate the fluorescence properties of MNCs. Compared to monometallic nanoclusters, the bimetallic structure of bimetallic nanoclusters can enhance the stability of nanoclusters and improve their fluorescence performance through the bimetallic synergistic effect [31,32]. Wang et al. achieved a significant enhancement in the luminescence quantum yield (approaching 100% at room temperature) of gold nanoclusters by sequentially adding Zn^{2+} and Ag^{+} [33]. Mi et al. synthesized Au/Ag bimetallic nanoclusters protected by dual ligands, using glutathione (GSH) and lysozyme as capping ligands [34]. The synthesized nanoclusters can be efficiently separated via isoelectric point precipitation. The purified Au/Ag bimetallic nanoclusters exhibit high sensing sensitivity toward H_2O_2 and hydroxyl radicals. Li et al. synthesized Au/Ag bimetallic nanoclusters using GSH as a template via a simple green hydrothermal method [35]. The as-prepared nanoclusters exhibit high quantum yield and stable FL performance based on aggregation-induced emission (AIE). The addition

of NaClO and Cu^{2+} disrupted the aggregation structure of the nanoclusters, leading to fluorescence quenching. Under optimal detection conditions, the probe achieved detection limits of 0.1 μM for free chlorine and 0.5 nM for Cu^{2+}.

These reported fluorescent probes are generally capable of achieving sensitive detection of target substances. However, most of these probes rely on precise measurement of fluorescence intensity using fluorescence spectrometers, which limits their practical application in on-site and rapid detection of such metal ions. Recently, smartphones have been widely adopted in on-site applications across various fields due to their portability and ease of operation, enabling powerful functionality through the installation of programs provided by third-party service providers. The visual detection of metal ions can be achieved through analysis of fluorescence images taken by smartphones [36]. In this work, a fluorescent probe based on Au/Ag bimetallic nanoclusters (GSH-Au/Ag NCs) was synthesized for the detection of Hg^{2+} and Cu^{2+}. The probe was upgraded as a ratiometric fluorescence sensor by mixing GSH-Au/Ag NCs and quinine sulfate. A method for detecting mercury and copper ions via smartphone-captured fluorescence images was developed, as illustrated in Scheme 1. The ratio (R/B) of fluorescence images exhibits a linear relationship with the concentrations of Hg^{2+} and Cu^{2+} in the ranges of 0.4–4 μM and 0.2–2 μM, respectively, enabling the determination of their concentrations by analyzing the RGB values from fluorescence images. This visual detection method is simple, convenient, rapid and cost-effective. It has broad application prospects in the field of metal ion detection.



Scheme 1. Preparation of GSH-Au/Ag NCs and the visual detection process of Hg^{2+} and Cu^{+2}.

2. Materials and Methods

2.1. Materials and Instruments

All chemical reagents were of commercial grade and were used directly without any further isolation or purification. Chloroauric acid ($AuCl_3{\cdot}HCl{\cdot}4H_2O$, AR, 98%), silver nitrate ($AgNO_3$, AR, 99.8%), quinine sulfate, sodium hydroxide (NaOH) and nitric acid (HNO_3) were purchased from Sinopharm Chemical Reagent Co., Ltd. (Shanghai, China). Glutathione in the reduced form (GSH, AR, 98%) was obtained from Macklin Inc. (Shanghai, China). All metal salts, including $NaNO_3$, $Mg(NO_3)_2$, $Zn(NO_3)_2$, $Mn(NO_3)_2$, $Ba(NO_3)_2$, $Ca(NO_3)_2$, $Co(NO_3)_2$, $Fe(NO_3)_3$, $Cu(NO_3)_2$, $Cd(NO_3)_2$, $Hg(NO_3)_2$, $Pb(NO_3)_2$, NaF, NaCl, Na_2CO_3, and Na_2SO_4, were supplied by Sinopharm Chemical Reagent Co., Ltd. Ultrapure water with a resistivity of 18.2 MΩ·cm was used throughout the experimental process and was from a Labonova Smart ultrapure water system (Think-lab, Boston, MA, USA).

Absorption spectra were collected with a two-beam UV-2600 ultra-violet spectrophotometer (Shimadzu, Kyoto, Japan). Fluorescence spectra were measured by an FS5 fluorescence spectrometer (Edinburgh Instrument, Livingston, UK), and the time-resolved spectra were obtained by an FLS920 steady-state/transient-state fluorescence spectrometer

(Edinburgh Instrument, Livingston, UK). TEM images were collected with a JEOL JEM 2010 microscope operating at 200 kV. X-ray photoelectron spectroscopy (XPS) measurements were performed with an ESCALAB 250Xi photoelectron spectrometer (Thermo Fisher Scientific, Waltham, MA, USA).

2.2. Synthesis of GSH-Au/Ag NCs

The synthesis of water-soluble fluorescent GSH-Au/Ag NCs refers to the literature report [37]. Typically, a freshly prepared aqueous solution of $AuCl_3$.HCl (25 mM, 0.6 mL) and a certain amount of $AgNO_3$ (50 mM, x mL) was first mixed with 6 mL of ultrapure water under gentle stirring (600 rpm) at room temperature, followed by the immediate addition of GSH (50 mM, 0.45 mL). After stirring for 5 min, the mixture solution was heated to 80 °C and continuously stirred for 12 h under gentle stirring (600 rpm). After the heating reaction was completed, a yellow and transparent aqueous solution of GSH-Au/Ag NCs with intense orange fluorescence was obtained. The ratio of Au:Ag could be controlled by changing the amount of $AgNO_3$. The synthesized GSH-Au/Ag NCs were stored at 4 °C and directly used without further purification.

2.3. Fluorescence Detection for Hg^{2+} and Cu^{2+}

The fluorescence of GSH-Au/Ag NCs can be significantly quenched by Hg^{2+} and Cu^{2+}. For the detection of Hg^{2+} and Cu^{2+}, a fluorescent probe solution was prepared by diluting GSH-Au/Ag NCs 100 times with phosphate buffer solution (PBS: 0.01 M, pH = 6.0). The fluorescence spectra were recorded before and after the addition of specific concentrations of Hg^{2+} or Cu^{2+}. Typically, 1.0 mL of Hg^{2+} or Cu^{2+} solutions at varying concentrations was added to 2.0 mL of the probe solution and shaken evenly. The mixture was incubated for ~30 min at room temperature. The resulting fluorescence spectra were recorded by a fluorescence spectrometer (λ_{ex} = 365 nm). Fifteen common ions, including Na^+, Mg^{2+}, Zn^{2+}, Mn^{2+}, Ba^{2+}, Ca^{2+}, Co^{2+}, Cd^{2+}, Pb^{2+}, Fe^{3+}, NO_3^-, F^-, Cl^-, CO_3^{2-}, and SO_4^{2-}, were chosen to assess the feasibility of the fluorescent probe.

2.4. Analysis of Real Water Samples

To evaluate the practical application of the fluorescent probe based on as-synthesized GSH-Au/Ag NCs, we used the probe to detect metal ions in tap water from our laboratory. For the detection procedure, the tap water was first filtered through a filter membrane with a pore size of 0.22 μm and then mixed with an equal volume of PBS (pH 6.0). The solution was then spiked with standard solutions of Hg^{2+} and Cu^{2+}. The real samples were measured using a similar method to that described above by using fluorescence spectra, and the reliability of this method was confirmed through ICP-MS analysis.

2.5. Visual Detection for Hg^{2+} and Cu^{2+}

For the visual detection of Hg^{2+} and Cu^{2+}, a colorimetric fluorescent probe solution was prepared by mixing quinine sulfate and GSH-Au/Ag NCs. Typically, 2 mL of GSH-Au/Ag NCs diluted 50-fold with PBS (0.01 M, pH = 6.0) was mixed with 20 μL of quinine sulfate (100 μM). Then, 1.0 mL of Hg^{2+} or Cu^{2+} solutions at varying concentrations was added and shaken evenly. After incubating for ~30 min at room temperature, the mixture solutions were transferred to a 3 mL quartz cuvette and, subsequently, fluorescent photographs were taken by a smartphone under a 365 nm UV lamp (HUAWEI nova Pro, HUAWEI Inc., Shenzhen, China). The photo-taking parameters were set as follows: ISO-3200, S-0.5S, EV-0, and F-1.8. Color information (RGB values) was obtained by calculating the fixed image area through MATLAB (R2018b). A physical image of the testing device is shown in Figure S1.

3. Results

3.1. Synthesis and Characterizations of GSH-Au/Ag NCs

Bimetallic metal nanoclusters exhibit enhanced fluorescence performance compared to single-metal nanoclusters, owing to the synergistic effects between the two metal components. Herein, water-soluble Au/Ag bimetallic nanoclusters (GSH-Au/Ag NCs) were synthesized through a facile one-pot heating process using glutathione (GSH) as the capping ligand. Typically, a certain ratio of AuCl3·HCl, $AgNO_3$ and GSH was mixed in water and stirred at 80 °C for 12 h. As the heating reaction proceeded, the mixture solution gradually changed from yellow to colorless, and then to orange-yellow. Finally, GSH-Au/Ag NCs with intense orange-red fluorescence were synthesized, as shown in Figure 1a. The emission spectrum shows a peak at ~610 nm with an optimal excitation wavelength of 275 nm. The Stokes shift is as large as 335 nm. This large Stokes shift is from the excited states relaxation of GSH-Au/Ag NCs via a p-band intermediate state (PBIS) [27,38–41]. The absorption spectrum presents a main peak at ~200 nm and two shoulder peaks at ~295 and ~400 nm. The absence of a plasmon resonance absorption peak indicates that no large metal nanoparticles were formed during the heating process, which is consistent with the TEM characterization results. As shown in Figure 1c, these as-synthesized metal nanoclusters have an ultrasmall size of approximately 1.45 nm. The addition of silver ions only affects the intensity of the emission peak without altering the position of the fluorescence peak, as shown in Figures 1b and S2. The optimal molar ratio of Au to Ag is 48:1; these nanoclusters were therefore employed in subsequent metal ion detection assays. After the introduction of silver ions, the absorption peaks shifted from 325 and 375 nm to 290 and 400 nm, implying a change in the electronic structure of the cluster (Figure S3). Notably, the emission peak of the doped clusters remains unchanged, with only a variation in intensity observed. This suggests that the energy levels of the emission centers remain unaltered. This can be well explained by our proposed ligand-centered photoluminescence theory [27,38]. The pH value is a critical parameter governing the synthesis of fluorescent nanoclusters [42]. As shown in Figures 1c and S4, fluorescent GSH-Au/Ag NCs can be synthesized under both acidic (pH~2.5) and alkaline (pH~10.0) conditions, while it is challenging to synthesize nanoclusters under neutral conditions (pH~7.0). GSH-Au/Ag NCs are formed through the reduction and growth of Au(I)-SG complexes with the doping of silver [43]. The pH condition influences the aggregation degree of the complexes and the reducing ability of the thiol groups. Under low pH conditions, the complexes aggregate tightly, facilitating the reduction and growth of Au(I). Under neutral conditions, the complexes are highly dispersed, which is unfavorable for the nucleation and growth of nanoclusters. Under alkaline conditions, the reducing ability of thiol groups is significantly enhanced, still enabling the reduction of Au(I) to form gold nanoclusters. Generally, gold nanoclusters synthesized under alkaline conditions are larger in size than those synthesized under acidic conditions, leading to a redshift in the emission wavelength, as illustrated in Figure S4. The fluorescence emission wavelength of the as-synthesized GSH-Au/Ag NCs is independent of the excitation wavelength (Figure S5), which can be explained by our previously proposed ligand-centered emission mechanism based on ligand interaction on the confined nanosurface [27,39,44]. The valence state of Au and Ag of the as-synthesized GSH-Au/Ag NCs was determined by XPS spectra. As shown in Figure 1d, two XPS peaks at ~368.0 and 374.0 eV were observed, which correspond to the $3d_{5/2}$ and $3d_{3/2}$ orbitals of zero-valent silver. The other two peaks at ~84.5 and 88.2 eV are assigned to the $4f_{7/2}$ and $4f_{5/2}$ orbitals of gold [37]. Each of these peaks could be deconstructed into two overlapped peaks. Typically, the former peak can be deconstructed into peaks centered at ~84.45 and ~85.20 eV, corresponding to Au(0) and Au(I), respectively. The XPS data indicates that the ratio of Au

to Ag in the synthesized GSH-Au/Ag NCs is ~12:1, which may be underestimated due to the surface-sensitive nature of XPS.

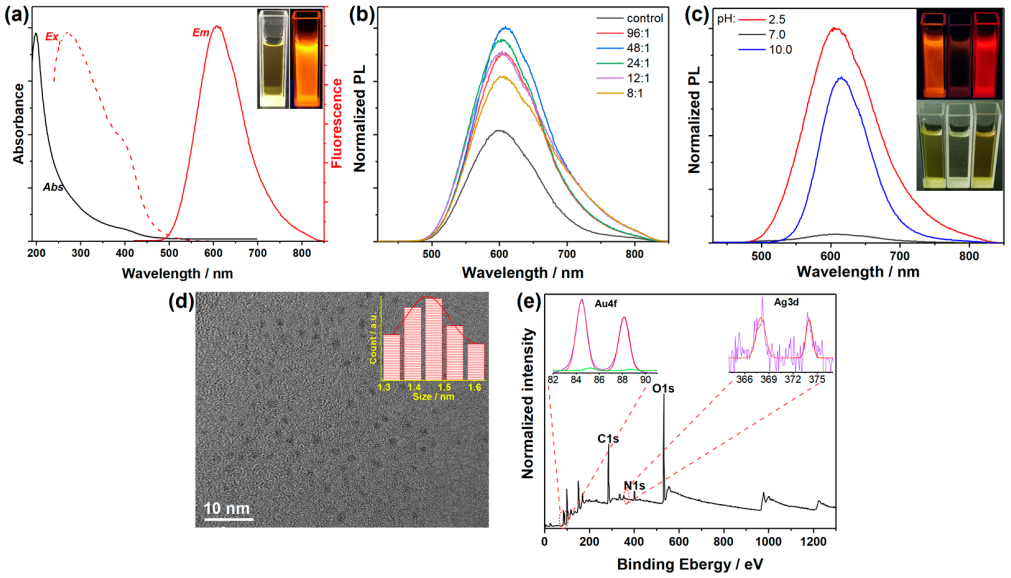


Figure 1. (**a**) Absorption (black solid line), excitation (red dotted line) and emission (red solid line) spectra of as-synthesized GSH-Au/Ag NCs. (Inset) Photographs of GSH-Au/Ag NCs under visible (left) and UV (right) light. (**b**) Fluorescence emission spectra of GSH-Au/Ag NCs with different ratios of Au to Ag. (**c**) Fluorescence emission spectra of GSH-Au/Ag NCs synthesized under different pH conditions. (Inset) Corresponding photographs under UV (**up**) and visible (**down**) light. (**d**) HRTEM image of as-prepared GSH-Au/Ag NCs (the histogram describes the statistical distribution of the cluster size). (**e**) XPS spectra of GSH-Au/Ag NCs.

The synthesized fluorescent GSH-Au/Ag NCs exhibit good photostability. As shown in Figure 2b, red line, the fluorescence of the clusters remains almost unchanged after being consecutively measured 360 times over 3 h. These properties, including a large Stokes shift and good photostability, make GSH-Au/Ag NCs a promising candidate for fluorescent probe materials. The as-synthesized GSH-Au/Ag NCs show a "on–off" response to Hg^{2+} and Cu^{2+}. As shown in Figure 2a, the fluorescence of the GSH-Au/Ag NCs was significantly quenched after the addition of Hg^{2+} and Cu^{2+}, and a "on–off" type fluorescent probe was designed.

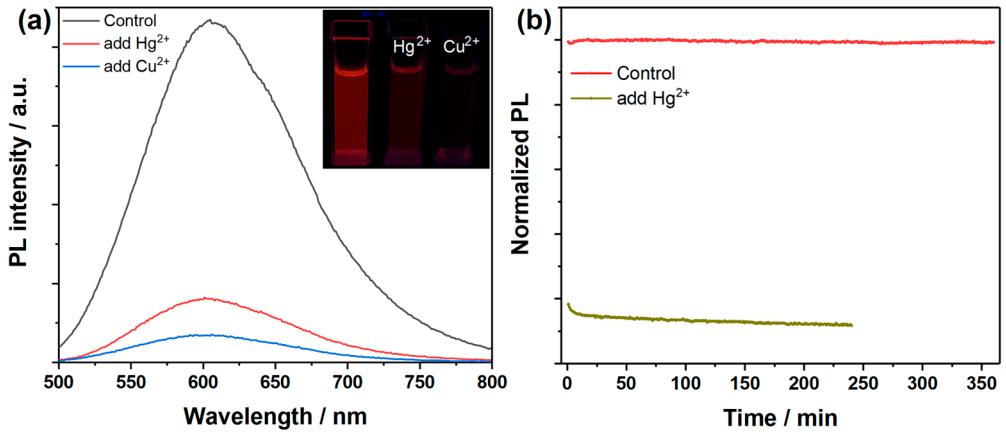


Figure 2. (**a**) Fluorescence emission spectra of GSH-Au/Ag NCs before and after adding Hg^{2+} and Cu^{2+} at a concentration of 5 μM. (Inset) Corresponding photographs under UV light. (**b**) The photostability and response time test of GSH-Au/Ag NCs to Hg^{2+}. The fluorescence intensity was continuously monitored at 30 s intervals.

3.2. Feasibility Analysis and Optimization of Experimental Conditions

The feasibility of the detection method was first analyzed. As shown in Figure 2a, in the absence of Hg^{2+} and Cu^{2+}, the GSH-Au/Ag NCs exhibit strong fluorescence with an emission peak at ~610 nm, whereas the fluorescence underwent a great decrease after the addition of 5 μM Hg^{2+} and Cu^{2+}. The fluorescence of the GSH-Au/Ag NCs reaches stability within a few minutes after the addition of mercury ions, as shown in Figures 2b and S6. These results indicate that Hg^{2+} and Cu^{2+} can efficiently quench the fluorescence of GSH-Au/Ag NCs. A fluorescent nanoprobe for the detection of Hg^{2+} and Cu^{2+} was developed based on ion-induced fluorescence quenching of GSH-Au/Ag NCs. The experimental conditions were further optimized to improve the detection performance of the probe, including the pH and concentration of the probe. As shown in Figures 3 and S7, the response of the probe to metal ions is highly dependent on pH conditions. With increasing pH, the quenching efficiency of Hg^{2+} on the probe's fluorescence first increases and then decreases, reaching an optimum at pH 6.0. For copper ions, the quenching efficiency rises rapidly with increasing pH and plateaus at pH 5.0. Consequently, the pH of the probe system was fixed at 6.0 using PBS buffer (0.01 M). In addition, the concentration of the probe can also influence its response performance. As shown in Figures S8 and S9, the quenching efficiency increases continuously with decreasing probe concentration. When the probe is diluted 200-fold, the quenching efficiency reaches 28 times (F_0/F). However, further increasing the dilution factor beyond 100-fold results in significantly reduced fluorescence intensity, leading to a poor signal-to-noise ratio in the spectra. Therefore, the probe used in subsequent detection procedures was diluted 100-fold.

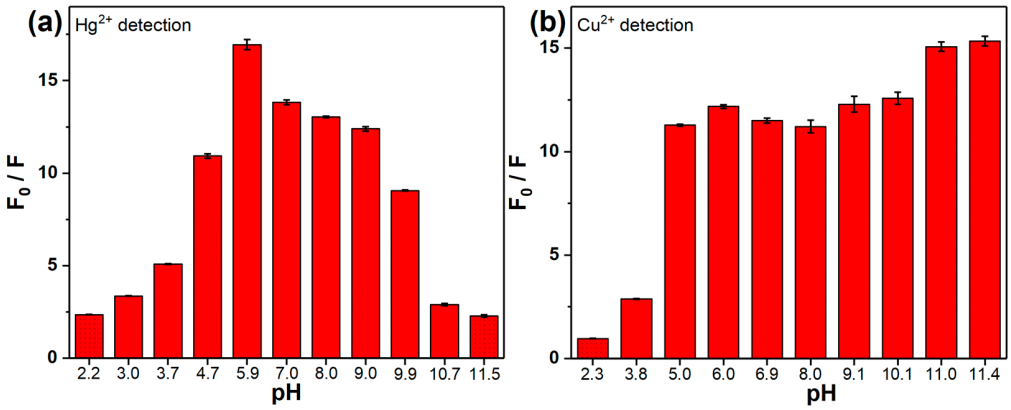


Figure 3. pH dependency of fluorescence quenching of GSH-Au/Ag NCs. F_0 and F are fluorescence intensities at 610 nm in the absence and presence of metal ions. Note that the concentration of Hg^{2+} in (**a**) is 10 μM and the concentration of Cu^{2+} in (**b**) is 5 μM.

3.3. Exploration of Detection Mechanism

In this section, we discuss the possible interaction mechanism between GSH-Au/Ag NCs and Hg^{2+} and Cu^{2+}. When investigating the influence of pH on optimizing detection conditions, it was found that the sensitivity of the GSH-Au/Ag NCs is highly pH-dependent. As shown in Figure 3, the response of the GSH-Au/Ag NCs to Hg^{2+} and Cu^{2+} gradually increases with the rise in pH. Note that the observed decrease in sensing ability of the GSH-Au/Ag NCs towards Hg^{2+} with increasing pH was attributed to the hydrolysis of Hg^{2+}, which forms insoluble mercury hydroxide ($Hg(OH)_2$) [45]. Also note that under low pH conditions (pH < 2.5), the GSH-Au/Ag NCs exhibit almost no response to Cu^{2+}, whereas Hg^{2+} can still cause a 50% quenching effect on the probe's fluorescence. In addition, the fluorescence quenched by Cu^{2+} can be fully restored by adding EDTA. In the case of Hg^{2+}, the addition of EDTA can only recover about 50% of the quenched fluorescence, as shown in Figure 4. These results indicate different quenching mechanisms

of the two metal ions. Based on relevant literature reports, the fluorescence quenching of GSH-Au/Ag NCs caused by Hg^{2+} is attributed to metal–metal interactions [46–48], whereas the fluorescence quenching induced by Cu^{2+} is primarily due to their binding with amino acids on the cluster surface [49]. The high affinity of the d^{10}-d^{10} metallophilic interaction between Au^{+} and Hg^{2+} leads to the effective fluorescence quenching of GSH-Au/Ag NCs [47]. Many literature reports indicate the high affinity of Cu^{2+} to the amino acids on the surface of clusters [50].

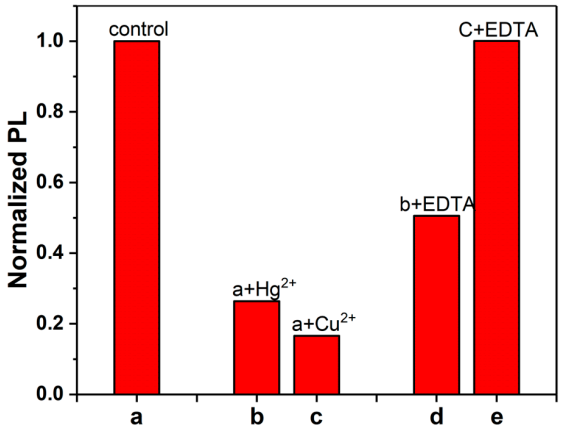


Figure 4. Fluorescence responses for GSH-Au/Ag NCs to Hg^{2+} and Cu^{2+} in the presence and absence of EDTA. Here, a, b, c, d and e indicate NCs, NCs + Hg^{2+}, NCs + Cu^{2+}, NCs + Hg^{2+} + EDTA, and NCs + Cu^{2+} + EDTA. Note that the dosage of EDTA is twice that of mercury and copper ions.

To further confirm the quenching mechanisms of Hg^{2+} and Cu^{2+} on the fluorescence of GSH-Au/Ag NCs, we conducted absorption spectroscopy and fluorescence lifetime measurements to investigate the optical properties of GSH-Au/Ag NCs in the presence of Hg^{2+} and Cu^{2+}. As shown in Figure 5a,b, the absorption of the GSH-Au/Ag NCs changes after the addition of Hg^{2+}, whereas it remains almost unchanged upon the addition of Cu^{2+}. In addition, although the fluorescence of the GSH-Au/Ag NCs is significantly quenched after the addition of Hg^{2+}, their fluorescence lifetime remains almost unchanged. Conversely, the fluorescence lifetime of the GSH-Au/Ag NCs significantly decreased upon the addition of Cu^{2+}, as shown in Figures 5c,d and S10. These results once again demonstrate that these two metal ions adhere to distinct fluorescence quenching mechanisms. Hg^{2+} ions bind to gold through metallophilic interactions, forming nonluminescent compounds, which fall under the category of static quenching mechanism. In contrast, Cu^{2+} ions interact with amino acids on the cluster surface, disrupting the assembled structure of surface ligands. This, in turn, affects the excited-state electron relaxation process of the clusters, leading to fluorescence quenching, and represents a dynamic quenching mechanism.

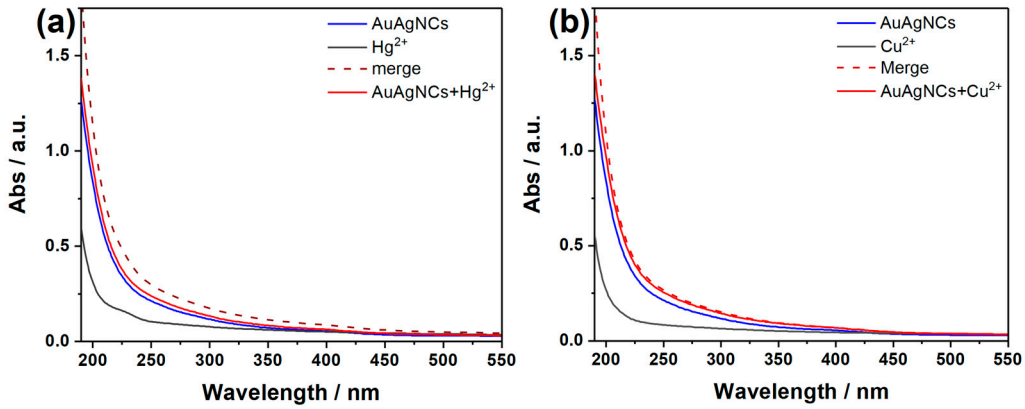


Figure 5. *Cont.*

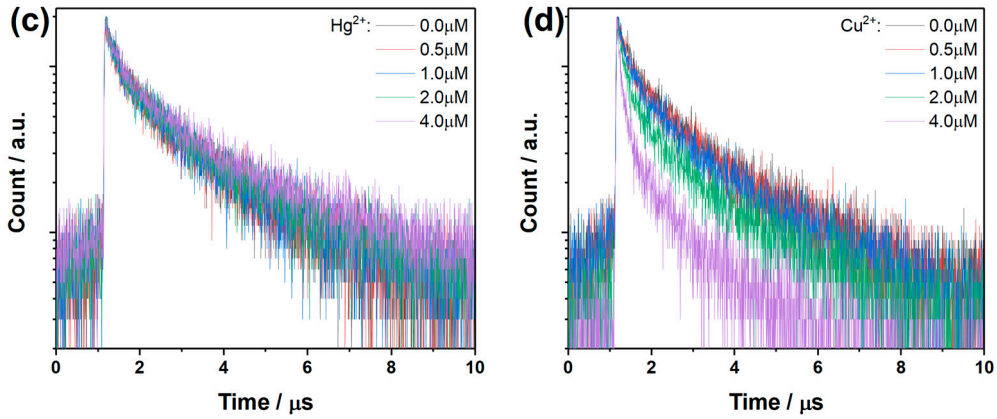


Figure 5. (**a**,**b**) Absorption spectra of GSH-Au/Ag NCs before and after mixing with Hg^{2+} and Cu^{2+}. (**c**,**d**) Time-resolved fluorescence spectra of GSH-Au/Ag NCs in the presence of Hg^{2+} and Cu^{2+} with different concentrations.

3.4. Selectivity Analysis of GSH-Au/Ag NCs

To evaluate the selectivity of the fluorescent probe, the response of the probe to other potential interfering ions in water, including Na^{+}, Mg^{2+}, Zn^{2+}, Mn^{2+}, Ba^{2+}, Ca^{2+}, Co^{2+}, Cd^{2+}, Pb^{2+}, Fe^{3+}, Cl^{-}, NO_3^{-}, CO_3^{2-}, and SO_4^{2-}, was investigated. The results are shown in Figure 6. Obviously, the fluorescence of the GSH-Au/Ag NCs was dramatically quenched in the presence of Hg^{2+} and Cu^{2+}. However, under the corresponding optimized detection conditions (the concentrations of all the interfering ions were fixed as 5 μM), the other ions exhibited negligible influence on the fluorescence of the GSH-Au/Ag NCs. This result indicates that this fluorescent probe can specifically detect Hg^{2+} and Cu^{2+}. In practical detection processes, Hg^{2+} and Cu^{2+} can be selectively masked by adding thiourea and EDTA, respectively, enabling the discrimination between Hg^{2+} and Cu^{2+}.

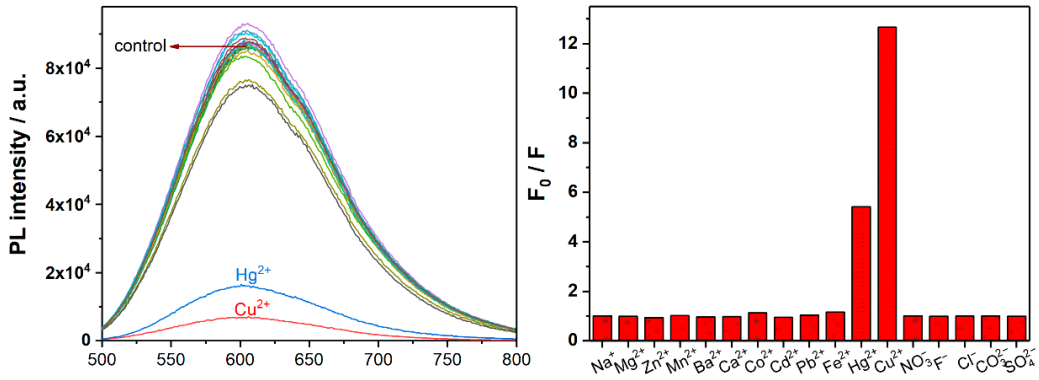


Figure 6. Selectivity study of the fluorescence probe based on GSH-Au/Ag NCs for the detection of Hg^{2+} and Cu^{2+}. The concentration of all ions was set as 5 μM.

3.5. Determination of Hg^{2+} and Cu^{2+} by GSH-Au/Ag NCs

A turn-off fluorescent probe was developed based on the on–off response of GSH-Au/Ag NCs to Hg^{2+} and Cu^{2+}. The calibration curves were constructed within the optimal experimental conditions by measuring the fluorescence spectra of GSH-Au/Ag NCs in the presence of Hg^{2+} and Cu^{2+} at varied concentrations. Figure 7a,c present the fluorescence spectra of the probe after the addition of 0–10 μM Hg^{2+} and Cu^{2+}, respectively. The corresponding relative fluorescence intensity (F/F_0, where F and F_0 are Hg^{2+} and Cu^{2+}) as a function of Hg^{2+} and Cu^{2+} concentrations is plotted in Figure 7b,d. An exponential decay in the fluorescence intensity of the GSH-Au/Ag NCs is evident with increasing Hg^{2+} and Cu^{2+} concentrations, featuring an initial sharp decline followed by a progressively slower

attenuation. The inset in Figure 7b shows that the relative fluorescence intensity of the nanoprobe exhibits a good linear relationship with the concentration of Hg^{2+} from 0.1 to 1.2 μM. The linear relationship is expressed as the regression equation y = 1.050 − 0.516x (R^2 = 0.990). The limit of detection (LOD) for Hg^{2+} was estimated as 40 nM according to the equation LOD = 3δ/k, where "δ" denotes the standard deviation of the blank measurement (n = 5) and "k" denotes the slope of the calibration curve. This detection sensitivity meets the detection requirements for Hg^{2+} in industrial wastewater, where the maximum allowable discharge concentration is 0.05 mg/L (250 nM, GB 8978-1996, China) [51]. The fluorescent probe also exhibits a linear response to Cu^{2+} within the same concentration range (0.1–1.2 μM), with the regression equation y = 0.996 − 0.586x (R^2 = 0.991) (inset of Figure 7d). The LOD for Cu^{2+} was calculated as 33 nM, which is far below the maximum permitted concentration of 1 mg/L (15.6 μM, GB 5749-2022, China) [52] in drinking water.

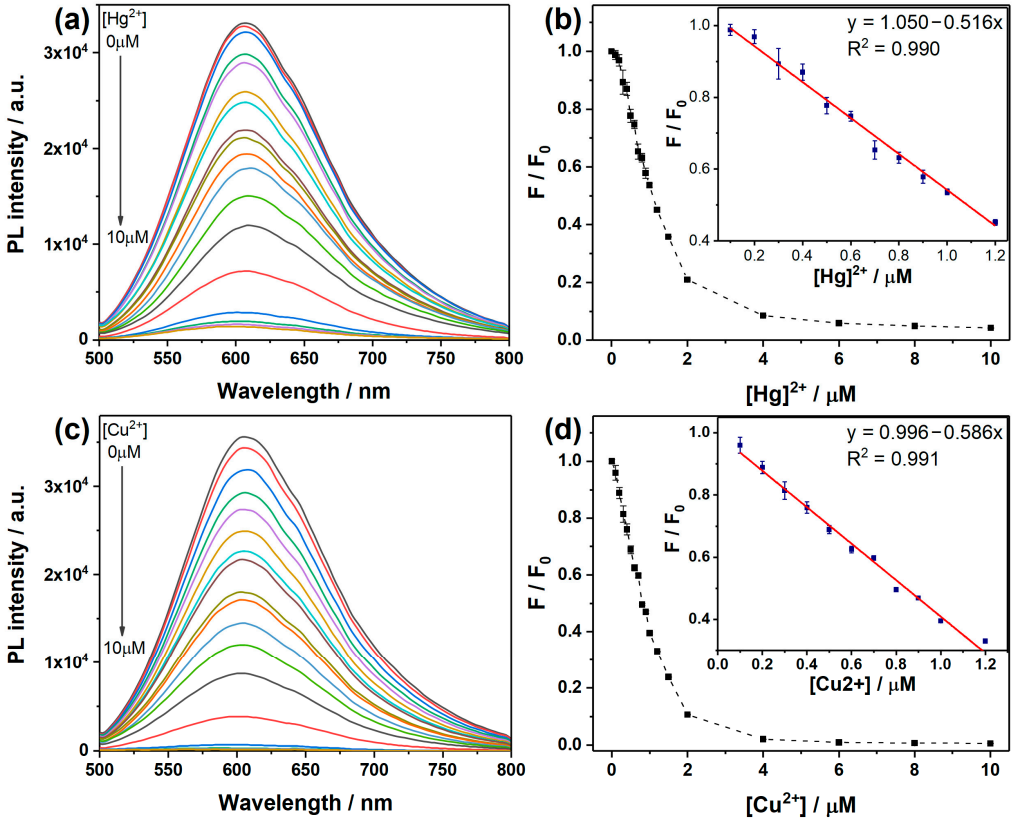


Figure 7. Fluorescence emission spectra of GSH-Au/Ag NCs in the presence of various concentrations of Hg^{2+} (**a**) and Cu^{2+} (**c**) from 0 to 10 μM. Relative fluorescence intensity of GSH-Au/Ag NCs in the presence of Hg^{2+} (**b**) and Cu^{2+} (**d**) from 0 to 10 μM. Inset, linear fitting result of the 0.1–1.2 μM fraction (y represents the relative intensity, and x represents the concentration of Hg^{2+} and Cu^{2+}).

3.6. Real Water Sample Analysis

To evaluate the practical application of the fluorescence probe in Hg^{2+} and Cu^{2+} detection, we further measured tap water (from Jiangnan University) with a standard addition method. The tap water sample did not cause any fluorescence quenching of the probe because the concentration of Hg^{2+} and Cu^{2+} in tap water is far below the detection limit of the probe. However, when different amounts of Hg^{2+} and Cu^{2+} were spiked into the real water, the fluorescence of the probe was significantly quenched, as shown in Figure S11. The determination results, along with recovery and RSD values of the spiked samples, are listed in Table 1. The recoveries of the spiked samples by the proposed method ranged from 89% to 104%, and all RSD values are less than 5%. The results indicated that

the fluorescent probe based on GSH-Au/Ag NCs is capable of conducting highly selective and sensitive detection of Hg^{2+} and Cu^{2+} in real water samples.

Table 1. Detection of Hg^{2+} and Cu^{2+} content in real samples.

Sample	FL Probe (nM)	ICP-MS (nM)	Added (nM)	Total Found (nM)	RSD (%)	Recovery (%)
1 (Hg^{2+})	Not detected	Not detected	400	416	2.4	104.0%
2			600	533	3.6	88.8%
3			800	797	0.5	99.6
4 (Cu^{2+})	Not detected	10 nM	400	408	5.0	102.0
5			600	605	1.2	100.8
6			800	791	1.3	98.9

3.7. Visual Detection of Hg^{2+} and Cu^{2+}

Fluorescent probes reported in the literature generally achieve sufficient sensitivity for the detection of Hg^{2+} and Cu^{2+} to meet practical requirements. However, most of these probes rely on precise measurement of fluorescence intensity using spectrofluorometers, which limits their application in on-site and rapid detection of heavy metal ions [28,53–55]. By capturing fluorescence images with smartphones and analyzing the color parameters of the images, on-site and rapid detection of metal ions can be realized. Herein, a ratiometric fluorescent probe was constructed by mixing quinine sulfate and GSH-Au/Ag NCs. As shown in Figure S12, a significant quenching of the red fluorescence of the GSH-Au/Ag NCs at ~610 nm is observed upon addition of Hg^{2+} and Cu^{2+}, while the blue fluorescence of quinine sulfate at ~446 nm remains unchanged. A ratiometric change in the intensities of red and blue fluorescence causes a visible color shift in the fluorescence images of the fluorescent probe under UV light. As shown in Figure 8, top photos, as the concentration of Hg^{2+} and Cu^{2+} gradually increases, the color of the probe progressively shifts from red to purple. We analyzed the RGB values of the images, and the results are presented in Figure 8. The R/G values of the fluorescence probe images exhibit a linear relationship with the concentrations of mercury ions (0.4–4 μM) and copper ions (0.2–2 μM). Smartphone-based third-party applications enable rapid on-site determination of Hg^{2+} and Cu^{2+} concentrations through photographic analysis.

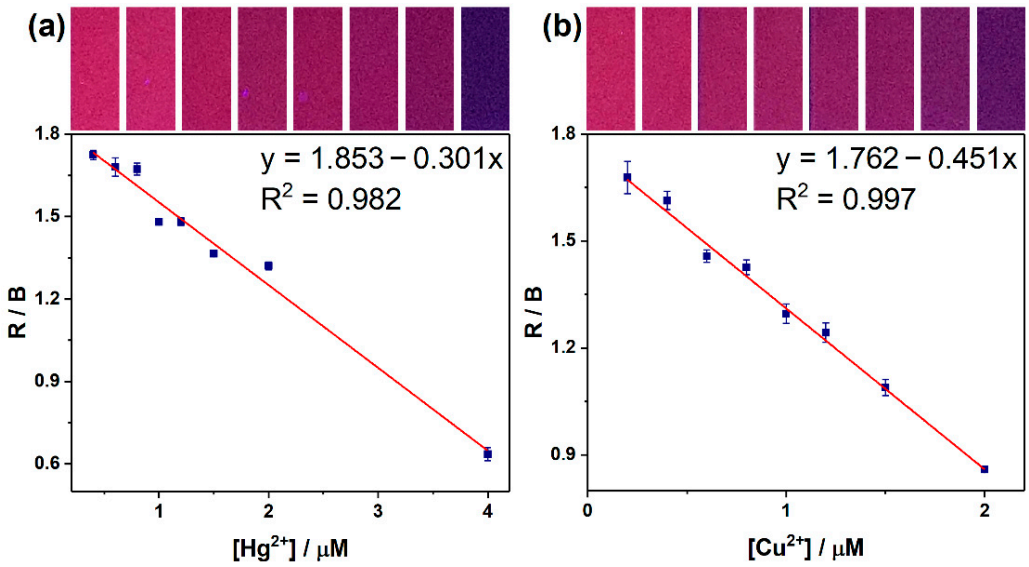


Figure 8. Plot of R/G value versus concentration of Hg^{2+} (**a**) and Cu^{2+} (**b**). The top pictures show corresponding photos that were taken with a smartphone under a 365 nm UV lamp.

The detection capabilities for Hg^{2+} and Cu^{2+} in this work and other reported fluorescent nanoprobes are compared in Table 2. The fluorescent probe, based on GSH-Au/Ag NCs, exhibits a comparable linear detection range and LOD. In addition, the sensing system can achieve visual detection of Hg^{2+} and Cu^{2+} with the assistance of a smartphone. The concentrations of Hg^{2+} and Cu^{2+} can be rapidly determined by analyzing images of the probe under UV light. It has great practical application in water environment monitoring as it enables on-site, rapid detection of metal ions.

Table 2. Comparison of recent optical methods for the determination of Hg^{2+} and Cu^{2+}.

Probe	Detected Ion	Visual Detection	Linear Range	LOD	Reference
Au NCs/CQDs	Hg^{2+} Cu^{2+}	No	0.83–77 μM -	0.36 μM -	[8]
Cu NCs	Hg^{2+} Cu^{2+}	No	0.04–60 μM -	20 nM -	[56]
Au NCs	Fe^{3+} Cu^{2+}	No	0.25–100 μM 0.25–25 μM	3.2μM 0.77 μM	[30]
Cu NCs/Tb-MOF	Hg^{2+} Cu^{2+}	No	- 1–30 μM	- 178 nM	[29]
Au NCs	Hg^{2+} Cu^{2+}	No	- 0.01–1.8 μM	- 8 nM	[57]
Au/Ag NCs/CDs	Hg^{2+} Cu^{2+}	No	20–2000 nM 20–600 nM	5 nM 7 nM	[45]
MOF/CdTe QDs	Hg^{2+} Cu^{2+}	yes	20–120 nM 62–620 nM	1 nM 4 nM	[11]
GSH-Au/Ag NCs	Hg^{2+} Cu^{2+}	Yes	0.1–1.2 μM 0.1–1.2 μM	40 nM 33 nM	This work

4. Conclusions

In conclusion, bimetallic fluorescent nanoclusters (GSH-Au/Ag NCs) were synthesized through a facile one-pot heating method. A fluorescent probe was designed based on as-synthesized GSH-Au/Ag NCs. The probe exhibits highly sensitive fluorescence quenching in response to Hg^{2+} and Cu^{2+}, with detection limits of 40 nM and 33 nM, respectively, over linear ranges of 0.1–1.2 μM. A ratiometric fluorescent probe was developed by mixing quinine sulfate and GSH-Au/Ag NCs. The ratio (R/B) of RGB values shows a linear relationship with concentrations of mercury ions (0.4–4 μM) and copper ions (0.2–2 μM), enabling rapid, visual detection through smartphone-based analysis. This visual detection method significantly reduces assay time and cost, providing a practical solution for on-site monitoring of heavy metals in water samples. The method offers a new paradigm for environmental monitoring applications, meeting the urgent demand for rapid, on-site detection of heavy metals.

Supplementary Materials: The following supporting information can be downloaded at https://www.mdpi.com/article/10.3390/chemosensors14040078/s1. Figure S1: The physical image of the visual detection device; Figure S2: 3D fluorescence spectra of as-synthesized GSH-Au/Ag NCs without AgNO3 and with AgNO3; Figure S3: UV−vis absorption spectra of as-synthesized GSH-Au/Ag NCs with different ratio of Au to Ag; Figure S4: Normalized fluorescence spectra of GSH-Au/Ag NCs synthesized under different pH conditions; Figure S5: Fluorescence emission spectra of GSH-Au/Ag NCs with varied excitation wavelength; Figure S6: The response time test of GSH-Au/Ag NCs to Hg^{2+}; Figure S7: Comparison of the fluorescence quenching degree of GSH-Au/Ag NCs by Hg^{2+} and Cu^{2+} under different pH conditions; Figure S8: Dilution-dependent fluorescence emission spectra of GSH-Au/Ag NCs at different dilution factors before and after adding Hg^{2+};

Figure S9: Fluorescence quenching efficiency of GSH-Au/Ag NCs at different dilution factors; Figure S10: Fluorescence spectra of GSH-Au/Ag NCs in the presence of Hg^{2+} and Cu^{2+} at different concentrations; Figure S11: Fluorescence emission spectra of fluorescent probe with the addition of tap water spiked with different concentration of Hg^{2+} and Cu^{2+}; Figure S12: Fluorescence spectra of as-developed ratiometric fluorescent probe before and after the addition of copper ions.

Author Contributions: Conceptualization, T.Y.; methodology, H.L., L.L. (Lei Li) and T.Y.; software, H.L. and L.L. (Lei Li); validation, H.L., L.L. (Lei Li) and T.Y.; formal analysis, H.L., L.L. (Lei Li) and T.Y.; investigation, T.Y.; resources, T.Y. and L.L. (Lei Li); data curation, H.L. and T.Y.; writing—original draft preparation, T.Y. and H.L.; writing—review and editing, T.Y., L.L. (Lei Li) and L.L. (Lang Liu); visualization, T.Y.; supervision, L.L. (Lang Liu); project administration, T.Y. and L.L. (Lang Liu); funding acquisition, T.Y. and L.L. (Lei Li). All authors have read and agreed to the published version of the manuscript.

Funding: This work was supported by the National Natural Science Foundation of China (22202085, 22004050).

Institutional Review Board Statement: Not applicable.

Informed Consent Statement: Not applicable.

Data Availability Statement: The original contributions presented in this study are included in the article/Supplementary Material. Further inquiries can be directed to the corresponding authors.

Conflicts of Interest: Author Hongbo Lin was employed by the company Changxin Xinqiao Storage Technology Co., Ltd. The remaining authors declare that the research was conducted in the absence of any commercial or financial relationships that could be construed as a potential conflict of interest.

References

1. Shu, Y.; Li, D.; Xie, T.; Zhao, K.; Zhou, L.; Li, F. Antibiotics-heavy metals combined pollution in agricultural soils: Sources, fate, risks, and countermeasures. *Green Energy Environ.* **2025**, *10*, 869–897. [CrossRef]
2. Huang, E.; Li, Y.; Ge, Y.; Dong, J.; Zhang, W. Early warning of soil and groundwater pollution by heavy metals: Progresses, perspectives and challenges. *Groundw. Sustain. Dev.* **2026**, *32*, 101567. [CrossRef]
3. Emamverdian, A.; Hasanuzzaman, M.; Ding, Y.; Barker, J.; Mokhberdoran, F.; Liu, G. Zinc Oxide Nanoparticles Improve Pleioblastus pygmaeus Plant Tolerance to Arsenic and Mercury by Stimulating Antioxidant Defense and Reducing the Metal Accumulation and Translocation. *Front. Plant Sci.* **2022**, *13*, 841501. [CrossRef] [PubMed]
4. De Silva, M.; Cao, G.; Tam, K.C. Nanomaterials for the removal and detection of heavy metals: A review. *Environ. Sci. Nano* **2025**, *12*, 2154–2176. [CrossRef]
5. Abo, L.D.; Areti, H.A.; Jayakumar, M.; Rangaraju, M.; Subashini, S. Nanobiomaterials-enabled sensors for heavy metal detection and remediation in wastewater systems: Advances in synthesis, characterization, and environmental applications. *Results Eng.* **2025**, *27*, 105694. [CrossRef]
6. Chauhan, S.; Dahiya, D.; Sharma, V.; Khan, N.; Chaurasia, D.; Nadda, A.K.; Varjani, S.; Pandey, A.; Bhargava, P.C. Advances from conventional to real time detection of heavy metal(loid)s for water monitoring: An overview of biosensing applications. *Chemosphere* **2022**, *307*, 136124. [CrossRef]
7. Yuan, L.; Liang, M.; Hummel, M.; Shao, C.; Lu, S. Rational Design Copper Nanocluster-Based Fluorescent Sensors towards Heavy Metal Ions: A Review. *Chemosensors* **2023**, *11*, 159. [CrossRef]
8. Chen, J.; Tian, R.; Li, D.; Sun, X.; Li, H.; Zhang, Y. Ratiometric fluorescence detection of Hg^{2+} based on gold nanocluster/carbon quantum dots nanohybrids. *Anal. Methods* **2024**, *16*, 884–891. [CrossRef]
9. Yu, F.; Xiang, H.; He, S.; Zhao, G.; Cao, Z.; Yang, L.; Liu, H. Gold nanocluster-based ratiometric fluorescent probe for biosensing of Hg^{2+} ions in living organisms. *Analyst* **2022**, *147*, 2773–2778. [CrossRef]
10. Luo, X.; Kong, J.; Xiao, H.; Sang, D.; He, K.; Zhou, M.; Liu, J. Noncovalent Interaction Guided Precise Photoluminescence Regulation of Gold Nanoclusters in Both Isolate Species and Aggregate States. *Angew. Chem. Int. Ed.* **2024**, *63*, e202404129. [CrossRef]
11. Yang, Y.; Liu, W.; Cao, J.; Wu, Y. On-site, rapid and visual determination of Hg^{2+} and Cu^{2+} in red wine by ratiometric fluorescence sensor of metal-organic frameworks and CdTe QDs. *Food Chem.* **2020**, *328*, 127119. [CrossRef]
12. Yin, S.; Leen, V.; Snick, S.V.; Boens, N.; Dehaen, W. A highly sensitive, selective, colorimetric and near-infrared fluorescent turn-on chemosensor for Cu^{2+} based on BODIPY. *Chem. Commun.* **2010**, *46*, 6329–6331. [CrossRef] [PubMed]

13. Altunay, N.; Yıldırım, E.; Gürkan, R. Extraction and preconcentration of trace Al and Cr from vegetable samples by vortex-assisted ionic liquid-based dispersive liquid–liquid microextraction prior to atomic absorption spectrometric determination. *Food Chem.* **2018**, *245*, 586–594. [CrossRef] [PubMed]
14. Zhang, X.-X.; Tang, S.-S.; Chen, M.-L.; Wang, J.-H. Iron phosphate as a novel sorbent for selective adsorption of chromium(iii) and chromium speciation with detection by ETAAS. *J. Anal. At. Spectrom.* **2012**, *27*, 466–472. [CrossRef]
15. Zhang, Y.; Shi, L.; Wu, Y. Determination of seven elements in manganese brass by inductively coupled plasma atomic emission spectrometry. *Metall. Anal.* **2017**, *37*, 40–44.
16. Aydin, F.A.; Soylak, M. Separation, preconcentration and inductively coupled plasma-mass spectrometric (ICP-MS) determination of thorium(IV), titanium(IV), iron(III), lead(II) and chromium(III) on 2-nitroso-1-naphthol impregnated MCI GEL CHP20P resin. *J. Hazard. Mater.* **2010**, *173*, 669–674. [CrossRef]
17. Bednar, A.J.; Kirgan, R.A.; Jones, W.T. Comparison of standard and reaction cell inductively coupled plasma mass spectrometry in the determination of chromium and selenium species by HPLC–ICP–MS. *Anal. Chim. Acta* **2009**, *632*, 27–34. [CrossRef]
18. Yu, X.; Chen, B.; He, M.; Wang, H.; Hu, B. 3D Droplet-Based Microfluidic Device Easily Assembled from Commercially Available Modules Online Coupled with ICPMS for Determination of Silver in Single Cell. *Anal. Chem.* **2019**, *91*, 2869–2875. [CrossRef]
19. Wang, X.; Liu, G.; Qi, Y.; Yuan, Y.; Gao, J.; Luo, X.; Yang, T. Embedded Au Nanoparticles-Based Ratiometric Electrochemical Sensing Strategy for Sensitive and Reliable Detection of Copper Ions. *Anal. Chem.* **2019**, *91*, 12006–12013. [CrossRef]
20. Bansod, B.; Kumar, T.; Thakur, R.; Rana, S.; Singh, I. A review on various electrochemical techniques for heavy metal ions detection with different sensing platforms. *Biosens. Bioelectron.* **2017**, *94*, 443–455. [CrossRef]
21. Zhang, J.; Li, S. Sensors for detection of Cr(VI) in water: A review. *Int. J. Environ. Anal. Chem.* **2019**, *101*, 1051–1073. [CrossRef]
22. Alam, P.; Leung, N.L.C.; Zhang, J.; Kwok, R.T.K.; Lam, J.W.Y.; Tang, B.Z. AIE-based luminescence probes for metal ion detection. *Coord. Chem. Rev.* **2021**, *429*, 213693. [CrossRef]
23. Kateshiya, M.R.; Desai, M.L.; Malek, N.I.; Kailasa, S.K. Advances in Ultra-small Fluorescence Nanoprobes for Detection of Metal Ions, Drugs, Pesticides and Biomarkers. *J. Fluoresc.* **2023**, *33*, 775–798. [CrossRef] [PubMed]
24. Wu, Y.-S.; Li, C.-Y.; Li, Y.-F.; Tang, J.-L.; Liu, D. A ratiometric fluorescent chemosensor for Cr^{3+} based on monomer–excimer conversion of a pyrene compound. *Sensor. Actuat. B Chem.* **2014**, *203*, 712–718. [CrossRef]
25. Kaviya, S.; Kabila, S.; Jayasree, K.V. Room temperature biosynthesis of greatly stable fluorescent ZnO quantum dots for the selective detection of Cr^{3+} ions. *Mater. Res. Bull.* **2017**, *95*, 163–168. [CrossRef]
26. Tang, J.; Zhang, J.; Zhang, W.; Xiao, Y.; Shi, Y.; Kong, F.; Xu, W. Modulation of red-light emission from carbon quantum dots in acid-based environment and the detection of chromium (III) ions. *J. Mater. Sci. Technol.* **2021**, *83*, 58–65. [CrossRef]
27. Yang, T.Q.; Peng, B.; Shan, B.Q.; Zong, Y.X.; Jiang, J.G.; Wu, P.; Zhang, K. Origin of the Photoluminescence of Metal Nanoclusters: From Metal-Centered Emission to Ligand-Centered Emission. *Nanomaterials* **2020**, *10*, 261. [CrossRef]
28. Benavides, J.; Quijada-Garrido, I.; García, O. The synthesis of switch-off fluorescent water-stable copper nanocluster Hg^{2+} sensors via a simple one-pot approach by an in situ metal reduction strategy in the presence of a thiolated polymer ligand template. *Nanoscale* **2020**, *12*, 944–955. [CrossRef]
29. Liu, P.; Hao, R.; Sun, W.; Lin, Z.; Jing, T. One-pot synthesis of copper nanocluster/Tb-MOF composites for the ratiometric fluorescence detection of Cu^{2+}. *Luminescence* **2022**, *37*, 1793–1799. [CrossRef]
30. Youn, J.; Kang, P.; Crowe, J.; Thornsbury, C.; Kim, P.; Qin, Z.; Lee, J. Tripeptide-Assisted Gold Nanocluster Formation for Fe^{3+} and Cu^{2+} Sensing. *Molecules* **2024**, *29*, 2416. [CrossRef]
31. Liu, J.; Zhao, R.; Wang, X.; Gao, X.; Zou, G. Mechanistic investigations into synergistically enhanced radiative-charge-transfer in Au-Ag bimetallic nanoclusters. *Chem. Commun.* **2020**, *56*, 5665–5668. [CrossRef] [PubMed]
32. Chen, T.; Yang, S.; Chai, J.; Song, Y.; Fan, J.; Rao, B.; Sheng, H.; Yu, H.; Zhu, M. Crystallization-induced emission enhancement: A novel fluorescent Au-Ag bimetallic nanocluster with precise atomic structure. *Sci. Adv.* **2017**, *3*, e1700956. [CrossRef] [PubMed]
33. Wang, X.; Zhong, Y.; Li, T.; Wang, K.; Dong, W.; Lu, M.; Zhang, Y.; Wu, Z.; Tang, A.; Bai, X. Sequential addition of cations increases photoluminescence quantum yield of metal nanoclusters near unity. *Nat. Commun.* **2025**, *16*, 587. [CrossRef] [PubMed]
34. Mi, W.; Tang, S.; Jin, Y.; Shao, N. Au/Ag Bimetallic Nanoclusters Stabilized by Glutathione and Lysozyme for Ratiometric Sensing of H_2O_2 and Hydroxyl Radicals. *ACS Appl. Nano Mater.* **2021**, *4*, 1586–1595. [CrossRef]
35. Li, D.; Wang, H.; Li, C.; Song, X.; Liu, X. GSH-AuAg NCs based fluorescent probe for multiple indicators in tap water: Free chlorine and copper ion. *J. Photoch. Photobiol. A* **2024**, *454*, 115712. [CrossRef]
36. Wang, H.; Yang, L.; Chu, S.; Liu, B.; Zhang, Q.; Zou, L.; Yu, S.; Jiang, C. Semiquantitative Visual Detection of Lead Ions with a Smartphone via a Colorimetric Paper-Based Analytical Device. *Anal. Chem.* **2019**, *91*, 9292–9299. [CrossRef]
37. Luo, Z.; Yuan, X.; Yu, Y.; Zhang, Q.; Leong, D.T.; Lee, J.Y.; Xie, J. From aggregation-induced emission of Au(I)-thiolate complexes to ultrabright Au(0)@Au(I)-thiolate core-shell nanoclusters. *J. Am. Chem. Soc.* **2012**, *134*, 16662–16670. [CrossRef]
38. Yang, T.; Shan, B.; Huang, F.; Yang, S.; Peng, B.; Yuan, E.; Wu, P.; Zhang, K. P band intermediate state (PBIS) tailors photoluminescence emission at confined nanoscale interface. *Commun. Chem.* **2019**, *2*, 132. [CrossRef]

39. Yang, T.; Dai, S.; Yang, S.; Chen, L.; Liu, P.; Dong, K.; Zhou, J.; Chen, Y.; Pan, H.; Zhang, S.; et al. Interfacial Clustering-Triggered Fluorescence-Phosphorescence Dual Solvoluminescence of Metal Nanoclusters. *J. Phys. Chem. Lett.* **2017**, *8*, 3980–3985. [CrossRef]
40. Yang, T.; Li, L.; Zhou, J.; Shan, B.; Gao, H.; Zhu, C.; Chen, G.; Zhang, K. Regulation of aggregation-induced emission properties of Ag(0)@Ag(I) rich-thiolate core-shell nanoclusters: Ligand assembly dominated. *J. Chem. Phys.* **2023**, *159*, 234702. [CrossRef]
41. Yang, T.; Zhou, J.; Shan, B.; Peng, B.; Li, L.; Gao, H.; Chen, G.; Zhang, K. Formation of Multiple Emission Centers of Gold Nanoclusters during the Aggregation-Induced Emission Process. *ACS Appl. Nano Mater.* **2023**, *6*, 17924–17931. [CrossRef]
42. Yao, Q.; Yu, Y.; Yuan, X.; Yu, Y.; Xie, J.; Lee, J.Y. Two-Phase Synthesis of Small Thiolate-Protected Au15 and Au18 Nanoclusters. *Small* **2013**, *9*, 2696–2701. [CrossRef] [PubMed]
43. Brinas, R.P.; Hu, M.; Qian, L.; Lymar, E.S.; Hainfeld, J.F. gold-nanoparticle-size-controlled-by-polymeric-au(i)-thiolate-precursor-size. *J. Am. Chem. Soc.* **2008**, *130*, 975–982. [CrossRef] [PubMed]
44. Yang, T.; Dai, S.; Tan, H.; Zong, Y.; Liu, Y.; Chen, J.; Zhang, K.; Wu, P.; Zhang, S.; Xu, J.; et al. Mechanism of Photoluminescence in Ag Nanoclusters: Metal-Centered Emission versus Synergistic Effect in Ligand-Centered Emission. *J. Phys. Chem. C* **2019**, *123*, 18638–18645. [CrossRef]
45. Babaee, E.; Barati, A.; Gholivand, M.B.; Taherpour, A.; Zolfaghar, N.; Shamsipur, M. Determination of Hg^{2+} and Cu^{2+} ions by dual-emissive Ag/Au nanocluster/carbon dots nanohybrids: Switching the selectivity by pH adjustment. *J. Hazard. Mater.* **2019**, *367*, 437–446. [CrossRef]
46. Lin, Y.-H.; Tseng, W.-L. Ultrasensitive Sensing of Hg^{2+} and CH_3Hg^+ Based on the Fluorescence Quenching of Lysozyme Type VI-Stabilized Gold Nanoclusters. *Anal. Chem.* **2010**, *82*, 9194–9200. [CrossRef]
47. Xie, J.; Zheng, Y.; Ying, J.Y. Highly selective and ultrasensitive detection of Hg^{2+} based on fluorescence quenching of Au nanoclusters by Hg^{2+}-Au^+ interactions. *Chem. Commun.* **2010**, *46*, 961–963. [CrossRef]
48. Niu, C.; Liu, Q.; Shang, Z.; Zhao, L.; Ouyang, J. Dual-emission fluorescent sensor based on AIE organic nanoparticles and Au nanoclusters for the detection of mercury and melamine. *Nanoscale* **2015**, *7*, 8457–8465. [CrossRef]
49. Durgadas, C.V.; Sharma, C.P.; Sreenivasan, K. Fluorescent gold clusters as nanosensors for copper ions in live cells. *Analyst* **2011**, *136*, 933–940. [CrossRef]
50. Marino, T.; Toscano, M.; Russo, N.; Grand, A. Structural and Electronic Characterization of the Complexes Obtained by the Interaction between Bare and Hydrated First-Row Transition-Metal Ions (Mn^{2+}, Fe^{2+}, Co2+, Ni^{2+}, Cu^{2+}, Zn^{2+}) and Glycine. *J. Phys. Chem. B* **2006**, *110*, 24666–24673. [CrossRef]
51. *GB 8978-1996*; Integrated Wastewater Discharge Standard. State Environmental Protection Administration of China: Beijing, China, 1994.
52. *GB 5749-2022*; Standards for Drinking Water Quality. State Administration for Market Regulation of China and Standardization Administration of China: Beijing, China, 2022.
53. Wu, Z.; Lu, T.; Hu, Y.; Mao, J.; Hu, X.; Qiu, J. Colorimetric and fluorescent AuNM nanosensors for mercury ion detection. *Coord. Chem. Rev.* **2025**, *537*, 216711. [CrossRef]
54. Pang, L.; Pi, X.; Zhao, Q.; Man, C.; Yang, X.; Jiang, Y. Optical nanosensors based on noble metal nanoclusters for detecting food contaminants: A review. *Compr. Rev. Food Sci. Food Saf.* **2024**, *23*, e13295. [CrossRef]
55. Luo, M.; Di, J.; Li, L.; Tu, Y.; Yan, J. Copper ion detection with improved sensitivity through catalytic quenching of gold nanocluster fluorescence. *Talanta* **2018**, *187*, 231–236. [CrossRef]
56. Luo, T.; Zhang, S.; Wang, Y.; Wang, M.; Liao, M.; Kou, X. Glutathione-stabilized Cu nanocluster-based fluorescent probe for sensitive and selective detection of Hg^{2+} in water. *Luminescence* **2017**, *32*, 1092–1099. [CrossRef]
57. Wen, R.; Li, H.; Chen, B.; Wang, L. Facile preparation of fluorescent gold nanocluster via polysaccharide-templated approach and its application for Cu^{2+} sensing. *Sens. Actuators B Chem.* **2017**, *248*, 63–70. [CrossRef]

Disclaimer/Publisher's Note: The statements, opinions and data contained in all publications are solely those of the individual author(s) and contributor(s) and not of MDPI and/or the editor(s). MDPI and/or the editor(s) disclaim responsibility for any injury to people or property resulting from any ideas, methods, instructions or products referred to in the content.